Kinetic study on clogging of a geothermal pumping well triggered by mixing-induced biogeochemical reactions

Luc Burté, Charles Cravotta, Lorine Bethencourt, Julien Farasin, Mathieu Pédrot, Alexis Dufresne, Marie-Françoise Gerard, Catherine Baranger, Tanguy Le Borgne, Luc Aquilina

Environmental Modeling

Kinetic study on clogging of a geothermal pumping well triggered by mixing-induced biogeochemical reactions

Luc Burte, Charles Cravotta, Lorine Bethencourt, Julien Farasin, Mathieu Pédrot, Alexis Dufresne, Marie-Françoise Gerard, Catherine Baranger, Tanguy Le Borgne, and Luc Aquilina

Environ. Sci. Technol., **Just Accepted Manuscript** • DOI: 10.1021/acs.est.9b00453 • Publication Date (Web): 30 Apr 2019

Kinetic study on clogging of a geothermal pumping well triggered by mixing-induced biogeochemical reactions

Luc Burté [†‡*], *Charles A. Cravotta III* [§], *Lorine Bethencourt* [†‖], *Julien Farasin* [†], *Mathieu Pédrot* [†], *Alexis Dufresne* [‖], *Marie-Françoise Gérard* [†], *Catherine Baranger* [‡], *Tanguy Le Borgne* [†], *Luc Aquilina* [†]

[†] Univ Rennes, CNRS, Géosciences Rennes - UMR 6118 - Av. Général Leclerc - F-35042 Rennes Cedex, France

[§] U.S. Geological Survey, 215 Limekiln Rd., New Cumberland, PA 17070, United States

[‖] Univ Rennes, CNRS, Écobio - UMR 6553 - Av. Général Leclerc - F-35042 Rennes Cedex, France

[‡]Antea Group, ZAC du Moulin 803 boulevard Duhamel du Monceau, Olivet, France

*Corresponding author: burte.luc@gmail.com

ABSTRACT

The sustainability of ground-source geothermal systems can be severely impacted by microbially mediated clogging processes. Biofouling of water wells by hydrous ferric oxide is a widespread problem. Although the mechanisms and critical environmental factors associated with clogging development are widely recognized, effects of mixing processes within the wells and time scales for clogging processes are not well characterized. Here we report insights from a joint hydrological, geochemical and metagenomics characterization of a geothermal doublet in which hydrous ferric oxide and hydrous manganese oxide deposits had formed as a consequence of mixing shallow groundwater containing dissolved oxygen and nitrate with deeper, anoxic groundwater containing dissolved iron (Fe^{II}) and manganese (Mn^{II}). Metagenomics identify distinct bacteria consortia in the pumping well oxic and anoxic zones, including autotrophic iron-oxidizing bacteria. Batch mixing experiments and geochemical kinetics modeling of the associated reactions indicate that Fe^{II} and Mn^{II} oxidation are slow compared the residence time of water in the pumping well; however, adsorption of Fe^{II} and Mn^{II} by accumulated hydrous ferric oxide and hydrous manganese oxide in the well bore and pump riser provides "infinite" time for surface-catalyzed oxidation and a convenient source of energy for iron-oxidizing bacteria, which colonize the surfaces and also catalyze oxidation. Thus, rapid clogging is caused by mixing-induced redox reactions and is exacerbated by microbial activity on accumulated hydrous oxide surfaces.

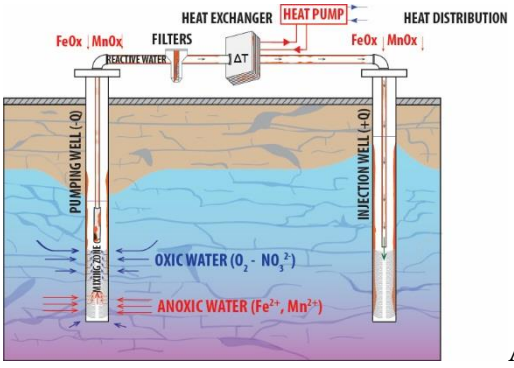

Abstract art (4.76 x 8.47 cm)

INTRODUCTION

Ground-source geothermal heating and cooling technologies can alleviate the use of fossil carbon energy and reduce greenhouse gas emissions to the atmosphere[1]. The technology of open-loop systems with direct transfer of energy from groundwater through a heat exchanger between pumping and injection wells (doublets) can be particularly cost-effective for heating and cooling buildings. Yet, the major issue associated with shallow geothermal doublets is the clogging of wells, exchangers, filters and other surface equipment by "biofouling" deposits that consist of mineral[2–5] and microbial[6–9] encrustations. Guaranteeing the sustainability of a groundwater heat pump system is challenging because of the rapidity at which such biofouling may appear, during the first year of exploitation in some cases observed by the authors. Clogging issues are also common in other groundwater sectors such as drinking water production[10–12], managed aquifer storage and recovery[13,14], and dewatering systems[15,16]. Although the processes at the origin of biogeochemical clogging have been described[17–19], the critical variables affecting hydrogeological and biogeochemical processes driving well biofouling are poorly characterized[20]. This is particularly true for unstable field parameters that can vary spatially and temporally with consequent effects on reaction development and rates, especially in the context of geothermal systems where neighboring geothermal doublets may exhibit different sensitivities to clogging, as illustrated in the present study.

Physical, chemical and microbiological processes contribute to clogging. Iron and manganese oxide (bio)mineralization is the most common cause of clogging encountered in water systems supplied by groundwater[21–23]. These clogging deposits form when anoxic groundwater containing dissolved iron (Fe^{II}) and manganese (Mn^{II}) mixes with water containing oxygen[2] or, possibly, nitrate[24] (Equations 1-7).

$$Fe^{II}\ Oxidation\ by\ Oxygen:\ Fe^{2+} + \frac{1}{4}O_2 + H^+ \rightarrow Fe^{3+} + \frac{1}{2}H_2O \quad (1)$$

$$Fe^{II}\ Oxidation\ by\ Nitrate:\ Fe^{2+} + \frac{1}{5}NO_3{}^- + \frac{6}{5}H^+ \rightarrow Fe^{3+} + \frac{1}{10}N_2 + \frac{3}{5}H_2O \quad (2)$$

$$Fe^{III}\ Hydrolysis:\ Fe^{3+} + 3H_2O \rightarrow Fe(OH)_3 \downarrow + 3H^+ \quad (3)$$

$$Mn^{II}\ Oxidation:\ Mn^{2+} + \frac{1}{4}O_2 + H^+ \rightarrow Mn^{3+} + \frac{1}{2}H_2O \quad (4)$$

$$Mn^{III}\ Hydrolysis:\ Mn^{3+} + 2H_2O \rightarrow MnOOH \downarrow + 3H^+ \quad (5)$$

$$Disproportionation:\ 2MnOOH + 2H^+ \rightarrow MnO_2 + Mn^{2+} + 2H_2O \quad (6)$$

$$Mn^{IV}\ reduction:\ MnO_2 + 2Fe^{2+} + 4H_2O \rightarrow 2Fe(OH)_3 + Mn^{2+} + 2H^+ \quad (7)$$

Mixing of oxic and anoxic groundwater can occur through different pathways: (1) oxygen-rich recharge water can infiltrate the aquifer due to pumping and mix with reduced groundwater near the well bore[12,25,26], (2) intermittent pumping can cause fluctuation of the water table and oxygenation of anoxic groundwater by air entrapment[27–31], (3) mixing of chemically heterogeneous water bodies in aquifers characterized by localized oxidizing condition (i.e. rich in O_2, NO_3^-) and reducing condition (i.e. rich in Fe^{2+}, Mn^{2+}) at different depths or spatially[2]. Despite the suspected role of mixing-induced biogeochemical reactions in clogging phenomena, field evidence demonstrating the impact is sparse[32–34]. Microbiological communities are known to be involved in clogging;[17–19,23,35] however, detailed information on where and when clogging can occur and potential competition with chemical oxidation is lacking for field conditions[36,37]. In the context of geothermal doublets, where fluid residence times in the geothermal loop are brief (typically few minutes), the mechanisms leading to observed rapid clogging of the system have not been quantified.

Field measurements, batch incubation experiments, and geochemical kinetics modeling were conducted to provide a quantitative framework for the prediction of clogging of geothermal wells. An interdisciplinary field campaign was conducted to characterize the key environmental variables

involved in mixing induced reactions that cause well clogging, including flow distribution and chemical heterogeneity within the well. A metagenomic study was carried out to investigate microbiological diversity and the potential roles of identified taxa in the chemical reactions. Batch incubation experiments, which included native microbes but excluded previously accumulated sorbent or biofilms, were used to demonstrate rates of change in solution chemistry that result from mixing of water from oxic and anoxic zones in the well. A geochemical kinetics model was then developed to simulate the mixing of the oxic and anoxic waters and observed decreases in dissolved iron and manganese concentrations in the simple batch system (homogeneous kinetics) and in the pumping well system where accumulated precipitate acts as a sorbent (heterogeneous kinetics) within the gravel pack, well bore, and pump. Field observations and modeling results that consider variations in microbial catalysis of Fe^{II} oxidation demonstrate how chemical heterogeneity and biogeochemical reactions promoted by pumping-induced mixing of oxic and anoxic waters can lead to rapid clogging of geothermal loops.

MATERIALS AND METHODS

Study area. The field site is a shallow geothermal doublet, DGSY, northeast of the city of Orléans (France) that began operation in October 2011, but eventually failed due to clogging. Technical information on well construction is summarized in **table SI.1** (supporting information). Doublet DGSY extracts groundwater from the limestone aquifer "Calcaire de Pithivier," which exhibits local karstification. The aquifer is unconfined and vulnerable to contamination as indicated by locally elevated concentrations of volatile organic compounds (1,2-dichloroethene, chloroform, trichloroethylene and methyl *tertiary*-butyl ether) and other unidentified organics that were documented before clogging. Operators report that during the first heating season (winter 2011-2012), the heat exchanger was clogged by reddish-brown deposits. Operators tried to

maintain the geothermal doublet, however, after multiple rehabilitation efforts, the well pump was removed in May 2016. The pump and the riser pipe were coated by slimy reddish-brown encrustations on the outer surface and underlying hard black deposits on the inner surface (**Figure SI.1** in supporting information). The deposits caused a reduction of 20 - 30% of the inner diameter of the riser pipe. Such biofouling was also likely to have accumulated in the well bore and, possibly, in the screen and gravel pack outside the well bore. The same layer of the targeted aquifer is used by another geothermal doublet located 750 m from DGSY. This doublet has been operated since 2008 without clogging issues.

In an attempt to understand the striking difference in sensitivity to clogging over a small distance, a series of interdisciplinary field campaigns was conducted during the spring and summer of 2017. In-situ measurements of physical and chemical characteristics were performed during static conditions and while pumped. The latter used a submersible pump (pumping rate of 16 m^3/h) placed above the top of the well screen of the pumping well P1 of DGSY to simulate the normal pumping condition.

Well logging. Video camera inspections were performed in each well of DGSY (pumping well P1 and injection well P2), allowing a direct in-situ visualization of clogging deposits. Vertical flowmeter logging was performed during pumping conditions in pumping well P1[38]. Flowmeter probes measured vertical movement of water in boreholes and allowed estimation of the permeability distribution along the well borehole[39]. To characterize the groundwater physico-chemical parameters in static and pumping conditions, multiparameter logs (pH, conductivity, dissolved O_2 (DO), Eh and temperature) were performed with a borehole probe in the pumping

well P1. Finally, a heat-pulse flowmeter probe was used to detect presence of vertical flows within pumping well P1 in static condition[40].

Chemical and metagenomic analysis. Water was sampled in pumping well P1 using a submerged well pump. Water was filtered through a 0.2-µm filter on site during sampling. Physico-chemical properties were obtained by using in-situ multiparameter probes placed in a continuous flow cell supplied by the well pump. Concentrations of major cations and anions, trace-element concentrations, dissolved organic carbon (DOC) and dissolved inorganic carbon (DIC) concentrations were analyzed following protocols described in Pédrot et al.[41]. Total Fe and Fe^{II} concentrations were measured and showed almost no difference, indicating that Fe is mainly Fe^{II}. An estimate of the relative abundances of all microorganisms was performed in the pumping well P1, by sampling of three replicates of 5 L of groundwater in the top and in the bottom of the well and sequencing of the total DNA by MiSeq run (Illumina INC). Analytical methods are detailed in **supporting information S2**.

Moist encrustations were sampled in April 2017 from the P1 pump riser that had been stored in a warehouse since May 2016. A small quantity of deposits was also sampled from the injection well P2. To characterize sampled deposits, scanning electron microscope (SEM) coupled with energy dispersive x-ray and major and trace-element analyses were performed.

Estimation of reactivity induced by mixing through batch experiments. As described in more detail in the Results & Discussion, two productive zones of chemically heterogeneous water (oxic, zone A and anoxic, zone H) were identified in the pumping well P1 during downhole logging. To quantify chemical reactions induced by mixing of the two types of produced water,

batch incubation experiments using the oxic and anoxic water were conducted. The batch experiment was designed to evaluate homogeneous oxidation kinetics involving native microbes, but excluding previously accumulated sorbents and biofilms that contribute to heterogeneous oxidation processes. Changes in the chemistry of three sets of water samples were evaluated: (1) oxic water from zone A, (2) anoxic water from zone H, and (3) a 50:50 mixture of the oxic and anoxic water. The water for these batch experiments was collected without atmospheric contact by pumping directly from well P1 at levels A and H into autoclaved glass bottles submerged within water-filled buckets. Ten bottles of each water type and the mixture (obtained by pumping from the oxic and anoxic zones simultaneously) were filled and then sealed with a septum while immersed. The sealed samples were incubated at 20 ºC in the laboratory. Over a period of 9 days, one bottle of each series (1 oxic, 1 anoxic and 1 suboxic mixture) was sacrificed daily to measure pH, DO, and concentrations of major ions and trace elements.

Geochemical model. To evaluate potential influences on clogging from various abiotic and biotic kinetic factors, as well as the role of adsorption on the attenuation of Fe^{II} and Mn^{II}, a geochemical model using PHREEQC[42] was employed. Details of the model construction are given by Cravotta[43] and summarized in the **supporting information S1 and S2**. Temperature corrections were automatically applied to constants for aqueous speciation, solubility, and kinetic rate expressions in the geochemical model. The thermodynamic data base, which includes kinetic rate expressions, is available with the model archive file in **supporting information S2**. The model simulates mixing of the oxic water and anoxic water of specified compositions in proportions pumped and considers kinetics of gas exchange and the oxidation of Fe^{II}, Mn^{II}, and organic carbon for three parallel or sequential steps. For the batch oxidation experiment, parallel reactions are

simulated for three different water samples: (1) oxic; (2) anoxic; and (3) mixed. The parallel model permits evaluation of the batch experiment as conducted, plus consideration of kinetic variables that may be important for more complex systems. For the more complex well clogging application, sequential steps simulate the generalized flow sequence at pumping well P1 of doublet DGSY: (1) gravel pack in annulus; (2) water column inside the well and screen; and (3) water within the pump and riser pipe to the injection head. Heterogeneous oxidation kinetics are computed for adsorbed Fe^{II} and Mn^{II}. The model computes the neutrophilic iron-oxidizing bacteria (FeOB) contribution to Fe^{II} oxidation as a function of the pH, DO, and adsorbed Fe^{II}.

RESULTS & DISCUSSION

Characteristics of the clogging deposits. Video revealed clogging deposits covering the inside surface of pumping well P1 from the top down to 33.4 m (6.54 m below the top of the well screen). The clogging deposits are reddish brown and became darker brown upward to the top of the well screen, possibly indicating variations in composition. Below 33.4 m, encrustations were not visible. Pumping tests at P1 showed no significant decrease of the well productivity since the first commissioning (initial values of specific capacity and those obtained during our study are 25 $m^3/h/m$ at 20 m^3/h and 48 $m^3/h/m$ at 16 m^3/h, respectively). The injection well P2 also had extensive deposits on the inner surface of the casing and well screen (**Figure 1**) and strong turbidity in the water column. The video of the injection well showed reddish flocs were easily mobilized from the well surfaces to the water column.

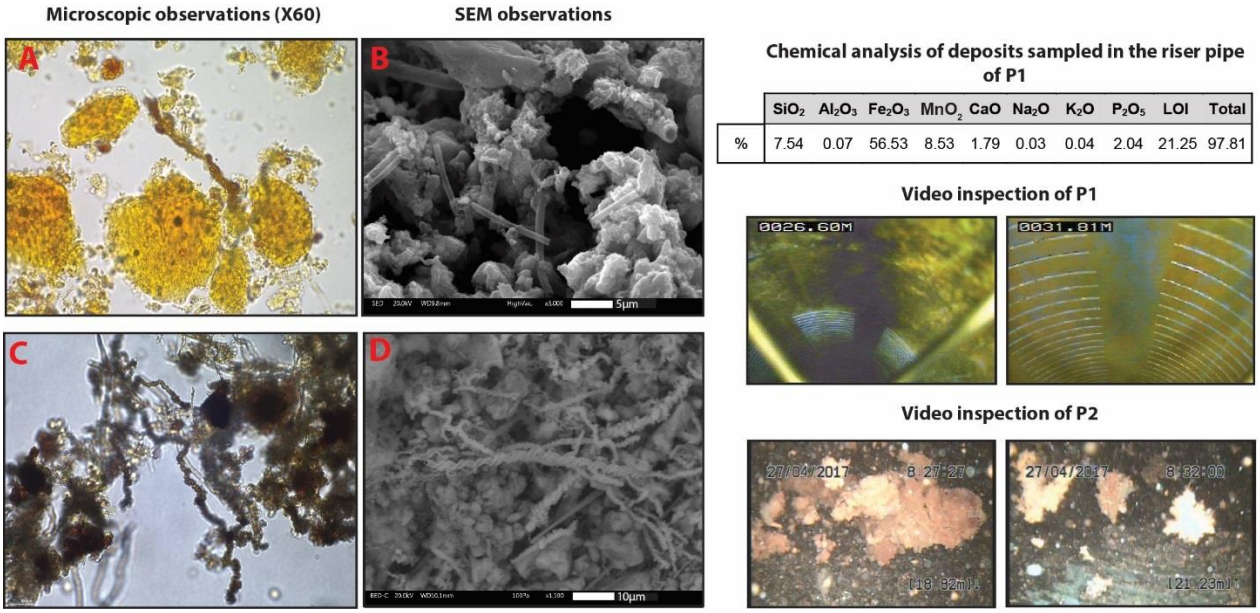

	SiO_2	Al_2O_3	Fe_2O_3	MnO_2	CaO	Na_2O	K_2O	P_2O_5	LOI	Total
%	7.54	0.07	56.53	8.53	1.79	0.03	0.04	2.04	21.25	97.81

186

187 **Figure 1.** Results of microscopic and SEM observations (**A - B**: deposits from the riser pipe of
188 pumping well P1, **C - D** : deposits from the injection well P2), chemical analysis of deposits
189 sampled in the riser pipe and pictures from the in -situ video inspection of geothermal doublet
190 DGSY, April 2017.

191 The moist deposits in the riser pipe consisted mainly of iron with smaller amounts of silica and
192 manganese, plus substantial organic carbon and structural water indicated by more than 20 percent
193 weight loss on ignition (LOI) (**Figure 1**). SEM and microscopic observations indicated the
194 presence of structures characteristic of FeOB growth (**Figure 1**): Hollow tubes may indicate
195 *Leptothrix* sp.[44]; twisted stalks may indicate *Gallionella* sp.[44].

196

197 **Physico-chemical characterization of the groundwater at pumping well P1.** The flowmeter
198 profile indicated nine productive zones along the well borehole (**Figure 2**). Two major productive
199 zones, between 26.1 to 27.4 m (zone A) and between 34.2 and 35.5 m (zone H) depth below the
200 top of the well screen, represented approximately 27.2 % and 41.1 % of the total flux, respectively,

during pumping. In static conditions (no pumping), heat-pulse flowmeter logs showed a downward flow (between 0.08 and 0.15 m/min) from the top of the well screen to the bottom of the well (exiting at zone I), indicating that the upper permeable zone has a higher hydraulic head than the lower permeable zone.

Dissolved oxygen (DO) profiles indicated significant redox heterogeneity (**Figure 2**). In static conditions, oxic characteristics (DO 1.6 - 3.3 mg/L) predominated above 34.3 m depth, while anoxic characteristics were detected between 34.3 and 34.5 m depth, corresponding to the upper part of zone H. The anoxic conditions coincided with the absence of nitrate (< 0.5 mg/L) between 33 and 35 m (**Figure 2**). Hypoxic conditions (DO < 1.2 mg/L) appeared below zone H. During pumping conditions, major inflows of oxygenated water were identified between 26.5 and 27.5 m (zone A) and between 28.5 and 29 m (zone C); however, at greater depths, DO concentrations remained less than 0.2 mg/L.

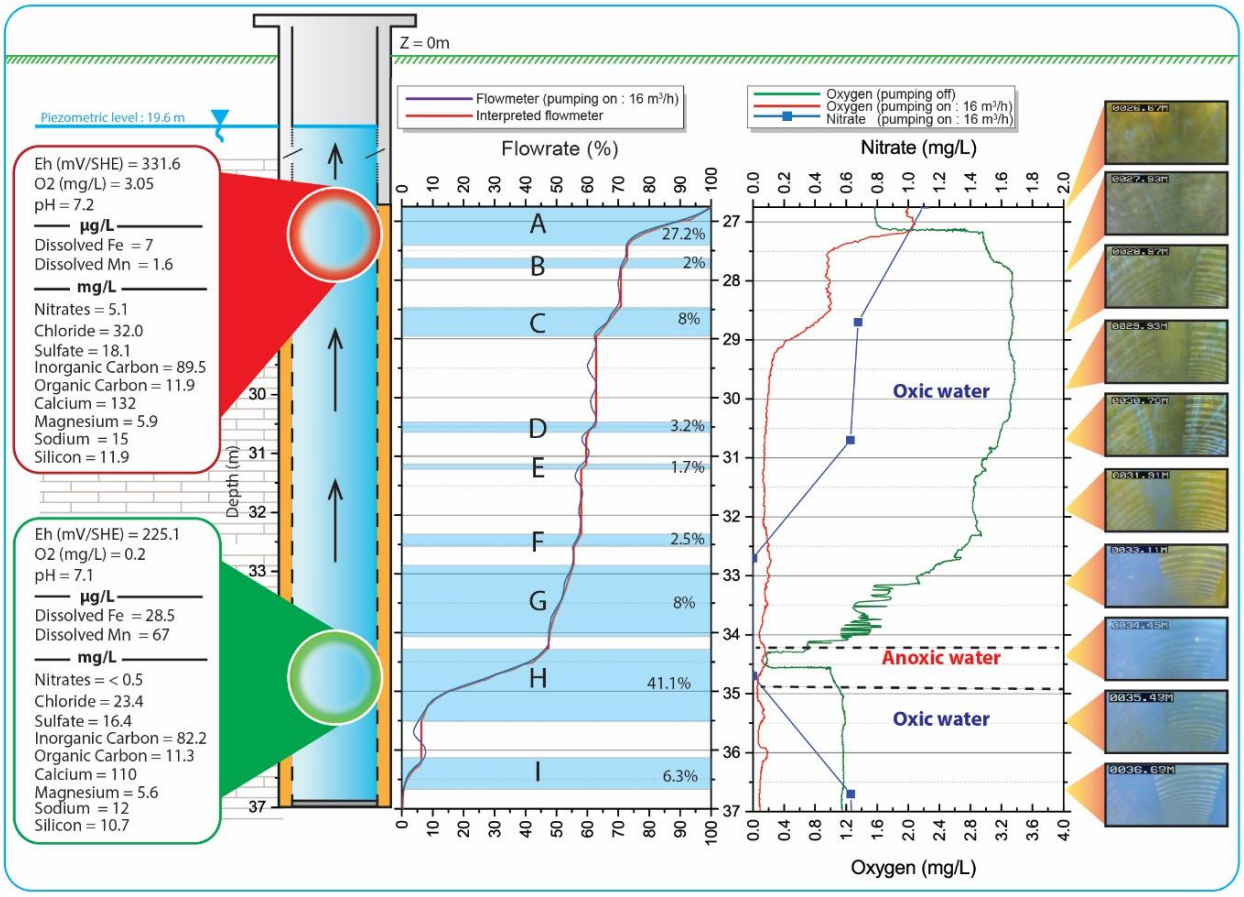

213

214 **Figure 2.** Vertical profile of dissolved nitrate (mg/L, pumping condition), dissolved oxygen
215 (mg/L, ambient and pumping condition), flow rate (%), video image of the pumping well, and
216 summary of chemical characteristics of the groundwater sampled from productive zones A (oxic)
217 and H (anoxic) in pumping well P1 of doublet DGSY during static conditions, April 2017.
218 Temperature, 12.6°C, is homogeneous along the well borehole.

219 The profiles of measured concentrations of iron and manganese (pumping condition) showed a
220 maximum near the anoxic zone. Measured concentration of dissolved iron is low compared to
221 previous analysis of total iron performed by the operator at the beginning of the operation
222 (0.1 mg/L in 2011 and 1.1 mg/L in 2014). Measured concentrations of other constituents (dynamic

223 conditions) showed similar vertical heterogeneity along the well screen. Thus, two chemically
224 distinctive waters were identified along the well screens of the pumping well P1 (**Figure 2**).

225 **Metagenomic analyses.** The bacteria taxa diversity along the well screen varied vertically
226 (**Figure 3**). Dominant bacteria of the oxic zone are of the *Pseudomonas* genus (e.g., *Pseudomonas*
227 *fluorescens*, *Pseudomonas veronii*) (70.75% of sequences). Globally, the identified bacterial
228 genera in the oxic zone could be involved in manganese oxidation (*Pseudomonas fluorescens*[45],
229 *Acinetobacter*[46], *Janthinobacterium*[47], *Variovorax*[48], *Caulobacter*[49], *Flavobacterium*[47,50,51],
230 *Bradyrhizobium*[52]) and nitrification (*Nitrospira*, *Nitrospina*). Communities of the anoxic zone
231 (**Figure 3)** are dominated by *Sphingomonadaceae*[53] (*Novosphingobium*, *Sphingobium*,
232 *Sphingopyxis* and *Sphingomonas* genera), especially known for degradation of polycyclic aromatic
233 hydrocarbons[54,55]. Iron reducing bacteria (FeRB) (*Rhodoferax, Geothrix*) are also detected in this
234 zone, as well as *Nitrospira* and *Nitrospina* genera. Moreover, despite the observation by electron
235 microscopy of characteristic structures of the best known FeOB, belonging to the *Gallionellaceae*
236 family (e.g., *Gallionella ferruginea*) and the *Leptothrix* genus (e.g., *Leptothrix ochracea*,
237 *Leptothrix discophora*) in the biofilm, sequences of these bacteria were not found at the two water
238 sampling points in the well. The metagenomics analysis reveals the microbial diversity of the two
239 main water bodies whose mixing induces clogging when operating the geothermal system. While
240 the bacteria involved in clogging process are naturally present in the aquifer, their relative
241 abundance is likely to be modified during the clogging process.

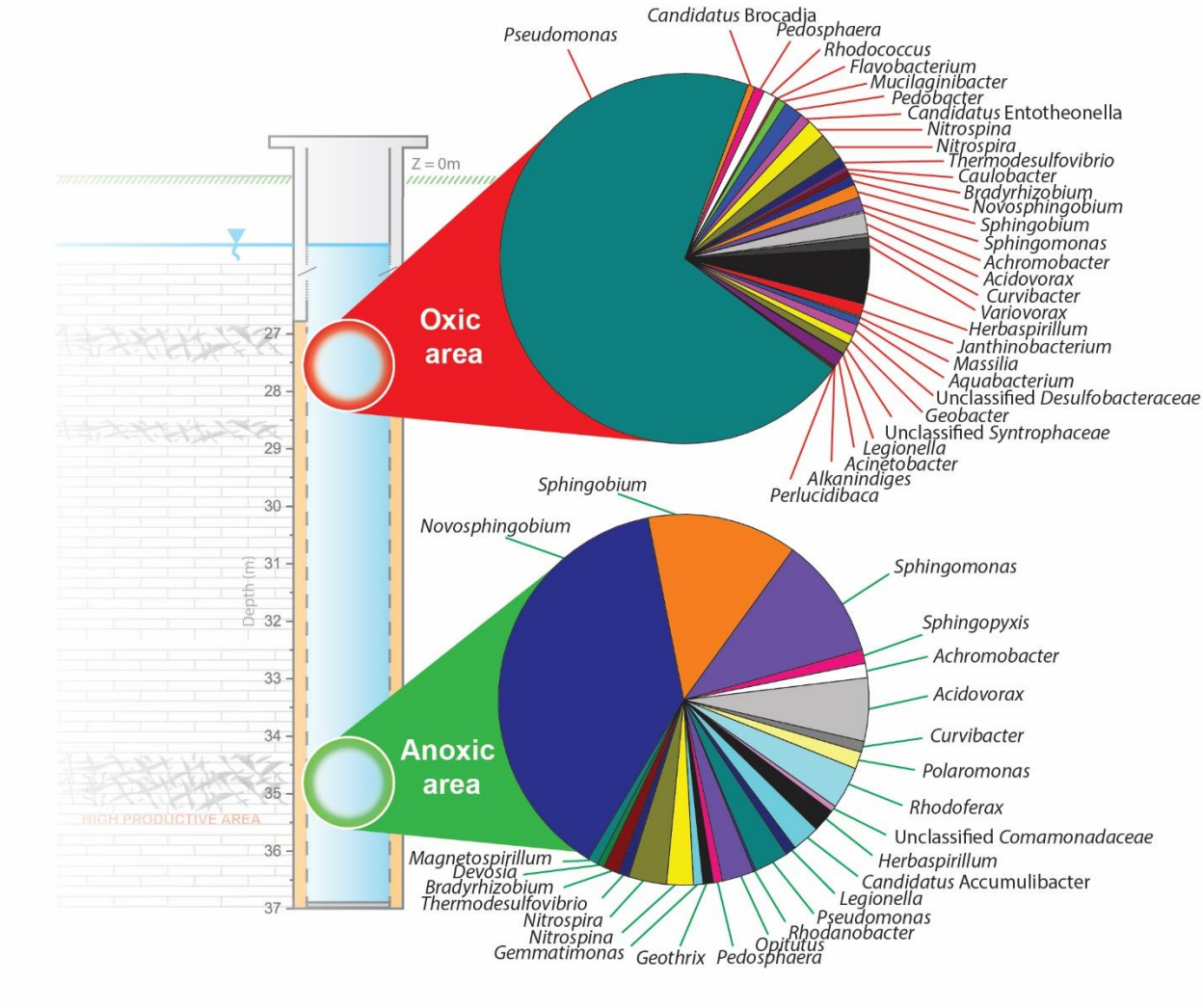

242

243 **Figure 3.** Relative abundances of bacterial genera present in the groundwater along the well

244 screens of P1, April 2017.

245

246

Experimental monitoring of reactive mixing process. Figures 4 and SI.4 (supporting information) show the observed changes in chemical concentrations of the oxic water, the anoxic water, and the mixed water extracted from pumping well P1 into sealed glass bottles and then monitored daily for 9 days in July 2017. Dissolved manganese concentrations were relatively stable within each series. In contrast, dissolved iron decreased to concentrations below detection and, therefore, is assumed to have been completely oxidized for the mixed water and oxic water. Concentrations of oxygen, nitrate, and dissolved organic carbon decreased in all three samples as shown in **Figure SI.4** (supporting information).

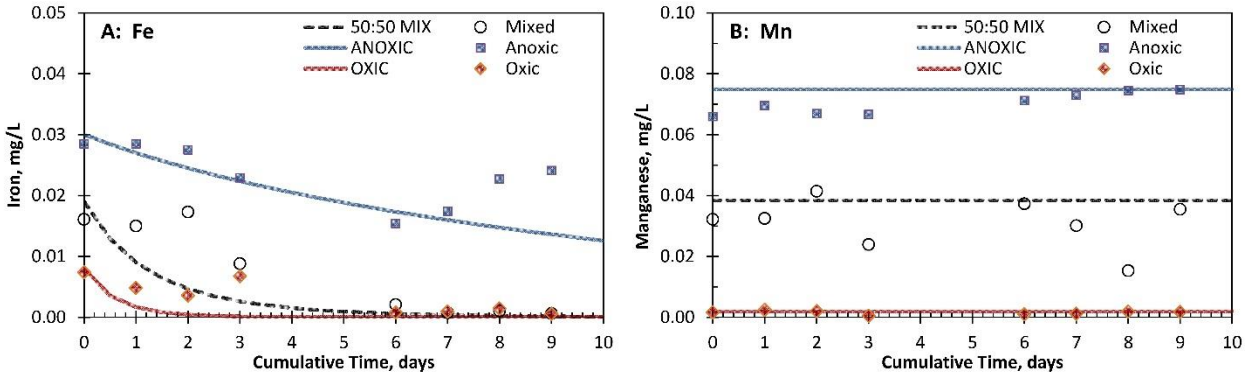

Figure 4. Time series of measured data (points) and PHREEQC simulation (lines) of chemical changes to oxic water, anoxic water, and suboxic water resulting from a 50:50 mixture from pumping well P1 for batch experiment.

Geochemical modeling of reactive mixing process. Figure 4 shows the model results (curves) compared to the empirical, batch mixing data (points). To simulate the suboxic mixed conditions, the oxic and anoxic waters were mixed in equal proportions (50:50), and the only sorbent considered was that produced by the oxidation and precipitation of initially aqueous Fe^{II} and Mn^{II} (autocatalytic oxidation). The model for the batch experiments demonstrates that the homogeneous Fe^{II} oxidation rate law[56], with adjustment for organic complexation of dissolved Fe, can account

for the observed Fe^{II} oxidation. Organic complexation of aqueous Fe^{II} and Fe^{III} by 1.5 mg/L humate slows down the simulated reaction rate by a factor 0.01, which is consistent with observed rates. Such organic complexation may result from naturally occurring organics, but probably results from locally elevated concentrations of manmade organic compounds (11-12 mg/L of uncharacterized DOC) at doublet DGSY as discussed below.

Figure 5 shows the results for simulations of sequential kinetic reactions within the pumping well system of the geothermal loop that could explain the rapid accumulation of clogging deposits during the 5-minute residence time. For these simulations, the proportion of oxic water and anoxic water was based on flowmeter measurements (respectively 59% and 41%). In contrast to the batch mixing experiment, where the only sorbent considered is that produced by abiotic plus biotic kinetic oxidation of dissolved Fe^{II} and Mn^{II}; the in-situ simulations consider added sorbent and show potential effects on attenuation of Fe^{II} and Mn^{II} by accumulated hydrous ferric oxide (HFO) and hydrous manganese oxide (HMO), plus catalytic activity by FeOB. For both scenarios shown in **Figure 5**, the amount of sorbent in the gravel pack was computed for a thickness of 0.01 μm, whereas that on well and pump was computed for a thickness of 1.0 μm. The accumulations inside the well column and pump were as thick as 0.01 m (**Figure SI.1** in supporting information); however, only a small fraction of that thickness (1.0 μm) is assumed to be in contact with water for surface reactions. Furthermore, the coating on the gravel pack was assumed to be 100% HFO (Fe), whereas that on the well and pump was 97.0% HFO, 2.9% HMO, and 0.1% hydrous aluminum oxide (HAO). Simulation results for the default FeOB oxidation rate (1X) (**Figures. 5A-5B**) produce the observed "biofouling" with iron-rich solids; increasing the FeOB oxidation rate by a factor of 10 (10X) greatly increases the accumulation of precipitate (**Figures. 5C-5D**). Additional simulation results shown as **Figure SI.5A-5J (**supporting information) demonstrate the

effects of different initial coatings (distribution and composition) as well as microbial catalysis (FeOB rates of 0X, 1X, and 10X) on Fe^{II} and Mn^{II} attenuation.

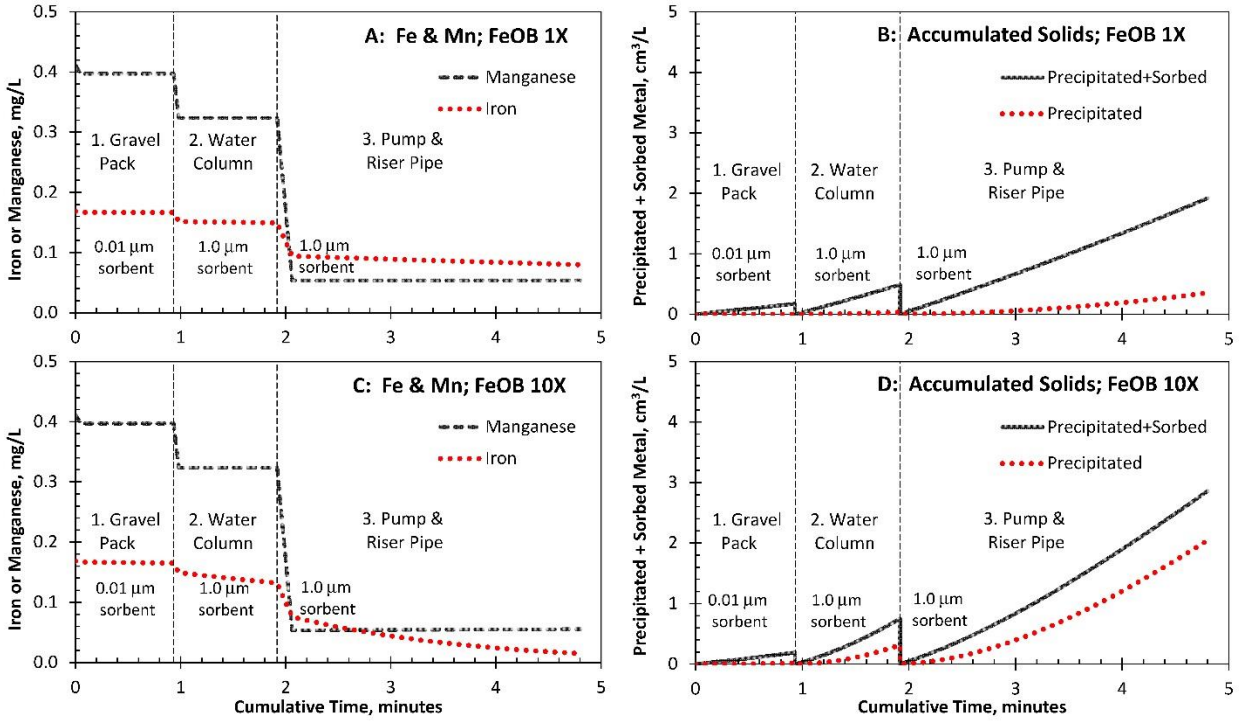

Figure 5. PHREEQC simulation of changes in dissolved Fe^{II} and Mn^{II} concentrations in mixed oxic (59%) and anoxic (41%) water and the consequent volume of precipitated+adsorbed metals produced by sequential kinetic and equilibrium speciation reactions in gravel pack, water column, and pump+riser pipe of geothermal loop pumping well P1. Results shown consider previously accumulated sorbent of varied mass (thickness 0.01 µm in gravel pack and 1.0 µm in well and pump+riser) and composition (100% HFO in gravel pack, and 97.0% HFO, 2.9% HMO, and 0.1% HAO in well and pump+riser) plus autocatalytic sorbent: A-B, default (1X) FeOB rate; C-D, enhanced (10X) FeOB rate.

Biogeochemical processes at the origin of clogging. Our investigations showed that doublet DGSY operates within a chemically heterogeneous aquifer (**Figure 2**) with distinct microbial

communities in the oxic and anoxic groundwater (**Figure 3**). In the anoxic zone, communities are dominated by *Novosphingobium*, *Sphingobium*, *Sphingomonas* genera, which do not appear in the oxic zones. Such communities are involved in the degradation of polycyclic aromatic hydrocarbons (PAHs)[24,57,58]. Thus, the anoxic conditions could result from oxygen consumption during bio-oxidation of PAHs that causes the release of dissolved metals from aquifer materials by reductive dissolution. Although no DOC distinction was observed between zone H and other zones, the DOC concentrations were assumed to be remnant of previous oxidation of organic pollutants. SEM analysis and microscopic observations of the deposits from the well pump indicate structures associated with FeOB (iron twisted stalks and iron hollow tubes; **Figure 1**). However, *Gallionella*, *Ferriphaselus* and *Leptothrix* genera were not identified in water samples collected along the well screen. This implies that biological structures in the clogging deposits may result from the activity of different FeOB (i.e. other *Comamonadaceae*[59] than the known *Leptothrix* bacteria, nitrate-dependent FeOB, or unidentified genera whose genome is not yet referenced), or the water samples may not represent the entire microbial community within biofilms on the well surfaces. Regardless, the positive identification of genera related to iron and manganese oxidation confirms that biological processes are probably involved in clogging processes. Further, once oxidized, Fe^{III} (as HFO) and Mn^{III-IV} (as HMO) may then serve as terminal electron acceptors for FeRB that decompose organic molecules. Sulfate-reducing bacteria (SRB) were observed at a low abundance that may indicate an insignificant contribution to the chemical processes. Although SRB activities have been reported in geothermal wells, redox levels in pumping well P1 were relatively high compared to other geothermal systems.

Mass balance of clogging deposits. The rapid clogging observed during 2011 operations indicates a massive and rapid accumulation of the oxide deposit. We estimated a hypothetical concentration of dissolved iron that could explain the rapid clogging based on the deposit distribution in the water system and the total recorded volume of water pumped since the beginning of operation. Observations of the pump column show a thickness of deposit of about 0.01 m. Assuming a constant thickness along the water system between the submerged well pump of P1 and the injection well P2, the estimated volume of clogging deposits is about 0.245 m^3. Note that this assumption does not consider the amount of deposits that may have precipitated within the well bore and gravel pack, nor the mobilized deposits that clogged the filter or that had been transported into the injection well P2. Chemical analysis (**Figure 1**) indicates that the dry deposit is composed of 56.5% Fe_2O_3 or 75.7% as $Fe(OH)_3$. Taking a bulk density of hydrous ferrous oxide[57] of 1.25 g/cm^3, the computed Fe^{2+} concentrations are approximately 0.37 mg/L, which is 12 times higher than measured concentrations in 2017 (**Figure 2**), but comparable to the concentrations (0.1 to 1.1 mg/L) reported by the operator at the beginning of operations in 2011. This result indicates that the chemical conditions in the aquifer could have evolved since 2011. In unconfined aquifers, concentrations of chemical species, including redox active species, have seasonal variations linked to recharge or discharge. Evidence of ambient downward vertical flow (infiltration of oxic groundwater from oxic zone to the underlying anoxic zone) was found within the pumping well during static conditions. Since the shutdown of the installation (May 2016), the invasion of oxic water may have caused a progressive oxidation of dissolved iron in the aquifer near the well. Hence, the chemical characteristics of the groundwater extracted from the anoxic zone during our study may differ from the initial conditions of the thermal pump operation in 2011.

Location of clogging processes. Video inspection of the pumping well shows extensive reddish-brown deposits in the upper part of the well and a lack of visible deposits in the anoxic zone. The visible deposits occurred from the piezometric surface at 19.6 m depth to the top of the anoxic zone at 33.4 m depth (**Figure 2**). Thus, clogging deposits appear to develop from the beginning of the geothermal loop where the aqueous Fe^{II} and Mn^{II} in the anoxic water mix with the oxic water during pumping. Presence of this clogging material along the geothermal loop (piping, filter, exchanger and injection well) can be explained by the transport of aqueous and solid forms of Fe and Mn along the flow path, with consequent interactions, explained below.

Geochemical modeling of the development of clogging deposits. The batch mixing experiment demonstrated that mixing of anoxic and oxic waters from the well resulted in more rapid and extensive Fe^{II} oxidation than achieved by solely the anoxic and oxic waters, while little if any Mn^{II} is attenuated (**Figure 4**). For the simulation of the batch experiment, the only sorbent was that formed by the in-situ oxidation of the initial Fe^{II} (0.03 mg/L and 0.008 mg/L) and Mn^{II} (0.075 and 0.002 mg/L) in the anoxic and oxic water, respectively. Complexing by 1.5 mg/L humate was considered to explain the slow rates of Fe^{II} oxidation. A concentration of 1.5 mg/L humate corresponds to approximately 6.5% of the measured, but uncharacterized DOC (11-12 mg/L) (**Figure 2**). Humate in the model may be considered a surrogate for natural organic matter (NOM) and manmade organic compounds that have varying capacities to form metal-organic complexes [60,61]. NOM contains between 40% and 60% C (fulvic acid 40% to 50% and humic acid 50% to 60%), whereas organic molecules of manmade origin have wide ranges in concentration of C (tetrachlorethylene 15% C to PAH 90% C). Rose and Waite (2003)[60] reported that Fe^{II}-NOM complex formation occurs on a similar time scale as Fe^{II} oxidation. Chen and Thompson (2018)[61]

demonstrated that complexation by natural organic acid substantially retarded Fe^{II} oxidation at 1% O_2, but had a negligible effect at 21% O_2. Without the simulated organic complexation of dissolved iron, the model predicted complete Fe^{II} attenuation from the mixed water within 24 hours.

The model simulating the mixing and sequential reactions in the pumping well (1) uses an initial concentration of 0.4 mg/L Fe^{II} in the anoxic water, consistent with the mass-balance computations, and (2) indicates that a rapid rate of chemical change, consistent with clogging observations, can take place primarily where previously accumulated HFO and HMO are available for reaction (**Figure 5**). Initial simulations indicate that simple mixing combined with homogeneous (autocatalytic) Fe^{II} oxidation, including microbial catalysis, has a negligible effect on Fe^{II} and Mn^{II} attenuation during the few minutes that water is retained in the well and pumping system (**Figure SI.5A-5B**). In this case, the reaction time for kinetic oxidation of Fe^{II} and Mn^{II} increases with distance from the mixing zone, favoring the accumulation of the precipitate further along the flow path between the pumping and injection wells. Such a simulation may mimic the early conditions in doublet DGSY. However, as the clogging deposit accumulated over time, the material began to function as an effective sorbent, catalyst for heterogeneous Fe^{II} and Mn^{II} oxidation, and substrate for microbial growth, all of which facilitated faster and more extensive accumulation of the oxide deposits (**Figures SI.5C-5J**).

The simulations show that if a uniform mass of HFO per liter of water is present throughout the gravel pack, well bore, and pump, most of the Fe^{II} and Mn^{II} removal takes place by adsorption processes within the gravel pack, which has a large surface area (**Figures SI.5C-5D**). However, based on our observations, the deposits were more extensive within the upper part of the well, pump, and riser pipe, and the observed materials contained a mixture of HFO and HMO. The simulation results shown in **Figures 5A-5D** (also shown as **Figures SI.5G-5J**) considered a 0.01X

393 smaller mass of sorbent in the gravel pack (0.01 μm thick, where mixing and oxidation are
394 negligible) compared to that within the well and pump (1.0 μm thick, where mixing and oxidation
395 take place), plus variable composition of sorbent (100% HFO in gravel pack; 97.0% HFO, 2.9%
396 HMO, and 0.1% HAO inside well and pump) combined with FeOB activity. Results for the
397 simulations with this heterogeneous sorbent distribution and composition and considering the
398 enhanced (10X) FeOB rate (**Figures 5C-5D** or **SI.5I-5J**) are consistent with the observed
399 biofouling of the pump and riser pipe and demonstrate that accumulated deposits within the upper
400 part of the well system combined with microbial catalysis can have a dramatic effect on attenuation
401 of Fe^{II} and Mn^{II} in that zone. It should be noted that the model default FeOB rate contribution (1X)
402 is an average factor of 20 times the abiotic heterogeneous Fe^{II} oxidation rate under optimum
403 conditions of near-neutral pH (6.5-7.5) and low DO (1.9-2.2 mg L^{-1}), whereas the enhanced rate
404 (10X) modeled is near the maximum FeOB rate reported for those conditions[35].
405 Increasing the percentage of HMO in the sorbent increases the attenuation of Mn^{II}. Because the
406 clogging material was heterogeneous, with the black (HMO) deposits overlain by reddish (HFO)
407 deposits, the simulations shown in **Figures 5A-5D** (and **Figures SI.5E-5J**) considered a lesser
408 amount of HMO in the surface layer (97.0% Fe, 2.9% Mn, and 0.1% Al) exposed to the
409 groundwater compared to the content reported for the riser pipe (87.93% Fe, 11.99% Mn, and
410 0.08% Al, expressed as the metals) (**Figure 1**). Simulations for a sorbent with that high HMO
411 content resulted in complete removal of dissolved Mn^{II}, which is inconsistent with observations.

412 The batch incubation experiments and geochemical kinetics models indicate that the rates of
413 homogeneous and heterogeneous Fe^{II} oxidation are relatively slow and inefficient at observed
414 near-neutral pH compared to the short residence time of water in the well bore and gravel pack,
415 even considering microbial catalysis. However, the field observations and modeling of in-situ

mixing and oxidation processes indicate that accumulated HFO, HMO, and biofilm on surfaces within the pump and riser pipe, the well bore, and, to a lesser extent, the surrounding gravel pack effectively bind Fe^{II} and Mn^{II}. The adsorbed metals have infinite time for oxidation and provide a convenient source of energy for FeOB that attach to the surfaces. For the modeled conditions within the well, concentrations of dissolved Fe^{II} were low compared to the accumulated HFO sorbent surface area. Despite continuous Fe^{II} adsorption, microbial oxidation of aqueous and (accumulated) adsorbed Fe^{II} replenishes the HFO sorbent. The metagenomics data indicate diverse microbial taxa and heterogeneous conditions in the aquifer; various organisms identified in oxic and anoxic zones could catalyze redox processes. The coupled adsorption and bio-oxidation processes facilitated by mixing of oxic and anoxic waters promote accumulation of Fe^{III}-Mn^{III-IV} precipitate and can thus trigger rapid clogging of pumping wells, despite relatively low concentrations of dissolved oxygen, Fe^{II} and Mn^{II} and short retention times of the groundwater in the well and plumbing system. In addition to restricting flow through the zone of accumulation, scour and transport of precipitated solids could explain rapid clogging of the filter at the heat exchanger within a few hours after a restarting of pumping.

The physical and biogeochemical reaction mechanisms described in this study may have a broad relevance for groundwater extraction systems where pumping induces mixing of oxic (O_2/NO_3 rich) and anoxic (Fe^{II}/Mn^{II} rich) groundwaters or introduces oxygenated air into the pumped water. To identify the risk and predict the appearance of clogging processes linked to Fe^{II} and Mn^{II} bio-oxidation, the hydraulic and chemical heterogeneity within the well should be characterized under static and pumping conditions at the start of shallow geothermal projects. In conventional geothermal system design, the feasibility of a geothermal operation is based on the chemical analysis of one water sample obtained at the end of a pumping test. Instead, a depth-oriented

sampling strategy, including in-situ water-quality logging, is warranted for identification of potentially oxidizing and reducing conditions along the well screen. In-situ characterization during ambient and dynamic conditions (coupled with flowmeter measurement) is necessary as the chemical signature of the water column inside the well is controlled by natural and induced fluxes. The initial precipitation of HFO and HMO deposits exacerbates additional accumulations, which implies a need for frequent rehabilitation procedures to avoid clogging. The intentional removal of deposits from the pumping well could involve a combination of physical and chemical applications. Adapted preventive methods (automatic back-washing filter, injection well equipped with back-washing pump) could be considered. In situations where clogging risk is significant, closed loop geothermal systems may be considered as an alternative to the open loop doublets.

ACKNOWLEDGMENTS

The authors thank managers of the studied geothermal doublet for granting permission to investigate the clogging phenomena and publish our results. This work was conducted as part of the research project “GEOCLOGGING,” which has been funded by the French Environment and Energy Management Agency (ADEME). We are grateful to Biogenouest Genomics and the Human & Environmental Genomics core facility of Rennes (Biosit/OSUR), especially Marine Biget and Sophie Michon-Coudouel, for the technical support concerning the metagenome sequencing. Helpful reviews of an early draft of the manuscript were provided by Dr. Oliver Opel of West Coast University of Applied Sciences, Fachbereich Technik, Heide Germany, and anonymous journal referees. Any use of trade, firm, or product names is for descriptive purposes only and does not imply endorsement by the U.S. Government.

SUPPORTING INFORMATION

Two files of supporting information (Word document and zip file) are offered. SI1 provides additional details on the characteristics of geothermal doublets DGSY, materials and methods (chemical and metagenomic analyses), and geochemical model development and application. Figures depicting results of geochemical simulations are also included. The model archive is available as a zip file, which includes the executable programs (parallel and sequential models), thermodynamic data base with rate expressions, and Excel files that summarize the simulation results and display the graphics used for figures in the main text and SI1.

REFERENCES CITED

(1) Famework Convention on Climate Change, United Nations. *Report of the Conference of the Parties on Its Twenty-First Session, Held in Paris from 30 November to 13 December 2015, Addendum Part Two: Action Taken by the Conference of the Parties at Its Twenty-First Session*; FCCC/CP/2015/10/Add.1; 2016.

(2) Possemiers, M.; Huysmans, M.; Anibas, C.; Batelaan, O.; Van Steenwinkel, J. Reactive Transport Modeling of Redox Processes to Assess Fe(OH)3 Precipitation around Aquifer Thermal Energy Storage Wells in Phreatic Aquifers. *Environ. Earth Sci.* 2016, *75* (8), 648. https://doi.org/10.1007/s12665-016-5398-7.

(3) García-Gil, A.; Epting, J.; Ayora, C.; Garrido, E.; Vázquez-Suñé, E.; Huggenberger, P.; Gimenez, A. C. A Reactive Transport Model for the Quantification of Risks Induced by Groundwater Heat Pump Systems in Urban Aquifers. *J. Hydrol.* 2016, *542*, 719–730. https://doi.org/10.1016/j.jhydrol.2016.09.042.

(4) Schneider, E. A. G.; García-Gil, A.; Vázquez-Suñè, E.; Sánchez-Navarro, J. Á. Geochemical Impacts of Groundwater Heat Pump Systems in an Urban Alluvial Aquifer with Evaporitic Bedrock. *Sci. Total Environ.* 2016, *544*, 354–368. https://doi.org/https://doi.org/10.1016/j.scitotenv.2015.11.096.

(5) Hähnlein, S.; Bayer, P.; Ferguson, G.; Blum, P. Sustainability and Policy for the Thermal Use of Shallow Geothermal Energy. *Energy Policy* 2013, *59*, 914–925. https://doi.org/https://doi.org/10.1016/j.enpol.2013.04.040.

(6) Gino, E.; Starosvetsky, J.; Kurzbaum, E.; Armon, R. Combined Chemical-Biological Treatment for Prevention/Rehabilitation of Clogged Wells by an Iron-Oxidizing Bacterium. *Environ. Sci. Technol.* 2010, *44* (8), 3123–3129. https://doi.org/10.1021/es903703v.

(7) Saripalli, K. P.; Meyer, P. D.; Bacon, D. H.; Freedman, V. L. Changes in Hydrologic Properties of Aquifer Media Due to Chemical Reactions: A Review. *Crit. Rev. Environ. Sci. Technol.* 2001, *31* (4), 311–349. https://doi.org/10.1080/20016491089244.

(8) Hand, V. L.; Lloyd, J. R.; Vaughan, D. J.; Wilkins, M. J.; Boult, S. Experimental Studies of the Influence of Grain Size, Oxygen Availability and Organic Carbon Availability on Bioclogging in Porous Media. *Environ. Sci. Technol.* 2008, *42* (5), 1485–1491. https://doi.org/10.1021/es072022s.

(9) Bonte, M.; Röling, W. F. M.; Zaura, E.; van der Wielen, P. W. J. J.; Stuyfzand, P. J.; van Breukelen, B. M. Impacts of Shallow Geothermal Energy Production on Redox Processes and Microbial Communities. *Environ. Sci. Technol.* 2013, *47* (24), 14476–14484. https://doi.org/10.1021/es4030244.

(10) Bustos Medina, D. A.; van den Berg, G. A.; van Breukelen, B. M.; Juhasz-Holterman, M.; Stuyfzand, P. J. Iron-Hydroxide Clogging of Public Supply Wells Receiving Artificial Recharge: Near-Well and in-Well Hydrological and Hydrochemical Observations. *Hydrogeol. J.* 2013, *21* (7), 1393–1412. https://doi.org/10.1007/s10040-013-1005-0.

(11) Houben, G. J. Iron Oxide Incrustations in Wells. Part 1: Genesis, Mineralogy and Geochemistry. *Appl. Geochem.* 2003, *18* (6), 927–939. https://doi.org/10.1016/S0883-2927(02)00242-1.

(12) van Beek, C. G. E. M.; Hubeek, A. A.; de la Loma Gonzalez, B.; Stuyfzand, P. J. Chemical and Mechanical Clogging of Groundwater Abstraction Wells at Well Field Heel, the Netherlands. *Hydrogeol. J.* 2017, *25* (1), 67–78. https://doi.org/10.1007/s10040-016-1469-9.

(13) Martin R. Clogging Issues Associated with Managed Aquifer Recharge Methods. Russel Martin (ed.) 2013.

(14) Brown, C. J.; Misut, P. E. Aquifer Geochemistry at Potential Aquifer Storage and Recovery Sites in Coastal Plain Aquifers in the New York City Area, USA. *Appl. Geochem.* 2010, *25* (9), 1431–1452. https://doi.org/10.1016/j.apgeochem.2010.07.001.

(15) Wang, J.; Sickinger, M.; Ciobota, V.; Herrmann, M.; Rasch, H.; Rösch, P.; Popp, J.; Küsel, K. Revealing the Microbial Community Structure of Clogging Materials in Dewatering Wells Differing in Physico-Chemical Parameters in an Open-Cast Mining Area. *Water Res.* 2014, *63*, 222–233. https://doi.org/10.1016/j.watres.2014.06.021.

(16) Weidner, C.; Henkel, S.; Lorke, S.; Rüde, T. R.; Schüttrumpf, H.; Klauder, W. Experimental Modelling of Chemical Clogging Processes in Dewatering Wells. *Mine Water Environ.* 2012, *31* (4), 242–251. https://doi.org/10.1007/s10230-012-0188-2.

(17) Georg Houben; Christoph Treskatis. *Water Well Rehabilitation and Reconstruction*; McGraw Hill Professional, Access Engineering, 2007.

(18) Cullimore, R. *Microbiology of Well Biofouling*, 1st Edition.; CRC press, 1999.

(19) Alford, G.; Cullimore, R. *The Application of Heat and Chemicals in the Control of Biofouling Events in Wells*, 1st Edition.; CRC press, 1998.

(20) Bonte, M.; Wols, B.; Maas, K.; Stuyfzand, P. Sources of Dissolved Oxygen in Monitoring and Pumping Wells. *Hydrogeol. J.* 2017, *25* (1), 55–66. https://doi.org/10.1007/s10040-016-1477-9.

(21) Schnieders, J. Well Blockage and Rehabilitation. In *Sterret, RJ (ed) Groundwater and wells*; Johnson Screens: New Brighton MN, 2007; pp 597–628.

(22) Driscoll, F. . Well and Pump Maintenance and Rehabilitation. In *Groundwater and wells*; Johnson Screens: St. Paul MN, 1986; pp 630–669.

(23) Eggerichs, T.; Otte, T.; Opel, O.; Ruck, W. K. L. Direct and Mn-Controlled Indirect Iron Oxidation by Leptothrix Discophora SS-1 and Leptothrix Cholodnii. *Geomicrobiol. J.* 2015, *32* (10), 934–943. https://doi.org/10.1080/01490451.2015.1039671.

(24) Appelo C. A. J.; Postma D. *Geochemistry, Groundwater and Pollution (2nd)*; A.A. Balkema Publishers: Leiden, The Netherlands, 2005.

(25) Menz, C. Oxygen Delivering Processes in Groundwater and Their Relevance for Iron-Related Well Clogging Processes–a Case Study on the Quaternary Aquifers of Berlin, Freie Universität Berlin, 2016.

(26) Farnsworth, C. E.; Voegelin, A.; Hering, J. G. Manganese Oxidation Induced by Water Table Fluctuations in a Sand Column. *Environ. Sci. Technol.* 2012, *46* (1), 277–284. https://doi.org/10.1021/es2027828.

(27) Kohfahl, C.; Massmann, G.; Pekdeger, A. Sources of Oxygen Flux in Groundwater during Induced Bank Filtration at a Site in Berlin, Germany. *Hydrogeol. J.* 2008, *17* (3), 571. https://doi.org/10.1007/s10040-008-0389-8.

(28) Williams, M. D.; Oostrom, M. Oxygenation of Anoxic Water in a Fluctuating Water Table System: An Experimental and Numerical Study. *J. Hydrol.* 2000, *230* (1), 70–85.

(29) Jia, M.; Bian, X.; Yuan, S. Production of Hydroxyl Radicals from Fe(II) Oxygenation Induced by Groundwater Table Fluctuations in a Sand Column. *Sci. Total Environ.* 2017, *584*, 41–47. https://doi.org/10.1016/j.scitotenv.2017.01.142.

(30) Holocher, J.; Peeters, F.; Aeschbach-Hertig, W.; Kinzelbach, W.; Kipfer, R. Kinetic Model of Gas Bubble Dissolution in Groundwater and Its Implications for the Dissolved Gas Composition. *Environ. Sci. Technol.* 2003, *37* (7), 1337–1343. https://doi.org/10.1021/es025712z.

(31) McLeod, H. C.; Roy, J. W.; Smith, J. E. Patterns of Entrapped Air Dissolution in a Two-Dimensional Pilot-Scale Synthetic Aquifer. *Groundwater* 2015, *53* (2), 271–281. https://doi.org/10.1111/gwat.12203.

(32) Englert, A.; Hubbard, S. S.; Williams, K. H.; Li, L.; Steefel, C. I. Feedbacks Between Hydrological Heterogeneity and Bioremediation Induced Biogeochemical Transformations. *Environ. Sci. Technol.* 2009, *43* (14), 5197–5204. https://doi.org/10.1021/es803367n.

(33) Li, L.; Steefel, C. I.; Williams, K. H.; Wilkins, M. J.; Hubbard, S. S. Mineral Transformation and Biomass Accumulation Associated With Uranium Bioremediation at Rifle, Colorado. *Environ. Sci. Technol.* 2009, *43* (14), 5429–5435. https://doi.org/10.1021/es900016v.

(34) Surasani, V. K.; Li, L.; Ajo-Franklin, J. B.; Hubbard, C.; Hubbard, S. S.; Wu, Y. Bioclogging and Permeability Alteration by L. Mesenteroides in a Sandstone Reservoir: A Reactive Transport Modeling Study. *Energy Fuels* 2013, *27* (11), 6538–6551. https://doi.org/10.1021/ef401446f.

(35) Eggerichs, T.; Opel, O.; Otte, T.; Ruck, W. Interdependencies between Biotic and Abiotic Ferrous Iron Oxidation and Influence of PH, Oxygen and Ferric Iron Deposits. *Geomicrobiol. J.* 2014, *31* (6), 461–472. https://doi.org/10.1080/01490451.2013.870620.

(36) Drescher, K.; Shen, Y.; Bassler, B. L.; Stone, H. A. Biofilm Streamers Cause Catastrophic Disruption of Flow with Consequences for Environmental and Medical Systems. *Proc. Natl. Acad. Sci. U. S. A.* 2013, *110* (11), 4345–4350. https://doi.org/10.1073/pnas.1300321110.

(37) Coyte, K. Z.; Tabuteau, H.; Gaffney, E. A.; Foster, K. R.; Durham, W. M. Microbial Competition in Porous Environments Can Select against Rapid Biofilm Growth. *Proc. Natl. Acad. Sci.* 2017, *114* (2), E161. https://doi.org/10.1073/pnas.1525228113.

(38) Le Borgne, T.; Bour, O.; Paillet, F. L.; Caudal, J.-P. Assessment of Preferential Flow Path Connectivity and Hydraulic Properties at Single-Borehole and Cross-Borehole Scales in a Fractured Aquifer. *Meas. Parameterization Rainfall Microstruct.* 2006, *328* (1), 347–359. https://doi.org/10.1016/j.jhydrol.2005.12.029.

(39) Paillet, F. L. Borehole Flowmeter Applications in Irregular and Large-Diameter Boreholes. *Non-Pet. Appl. Boreh. Geophys.* 2004, *55* (1), 39–59. https://doi.org/10.1016/j.jappgeo.2003.06.004.
(40) Le Borgne, T.; Paillet, F.; Bour, O.; Caudal, J. Cross-Borehole Flowmeter Tests for Transient Heads in Heterogeneous Aquifers. *Groundwater* 2006, *44* (3), 444–452. https://doi.org/10.1111/j.1745-6584.2005.00150.x.
(41) Pédrot, M.; Dia, A.; Davranche, M.; Gruau, G. Upper Soil Horizons Control the Rare Earth Element Patterns in Shallow Groundwater. *Geoderma* 2015, *239–240*, 84–96. https://doi.org/10.1016/j.geoderma.2014.09.023.
(42) Parkhurst, D. L.; Appelo, C. A. J. *Description of Input and Examples for PHREEQC Version 3—A Computer Program for Speciation, Batch-Reaction, One-Dimensional Transport, and Inverse Geochemical Calculations*; U.S. Geological Survey Techniques and Methods; book 6, chap. A43, 497 p; 2013; p 497.
(43) Cravotta, C. A. User-Friendly Geochemical Modeling to Evaluate Active and Passive Treatment for Coal Mine Discharges: Proceedings 39th Annual Meeting West Virginia Surface Mine Drainage Task Force : Morgantown; W.Va., West Virginia University, 2018.
(44) Kappler, A.; Emerson, D.; Gralnick, J. A.; Roden, E. E.; Muehe, E. M. Geomicrobiology of Iron. In *Ehrlich's geomicrobiology*; CRC press: 6000 Broken Sound Parkway NW, Suite 300, 2016; pp 343–399.
(45) Okazaki, M.; Sugita, T.; Shimizu, M.; Ohode, Y.; Iwamoto, K.; de Vrind-de Jong, E. W.; de Vrind, J. P.; Corstjens, P. L. Partial Purification and Characterization of Manganese-Oxidizing Factors of Pseudomonas Fluorescens GB-1. *Appl. Environ. Microbiol.* 1997, *63* (12), 4793–4799.
(46) Hosseinkhani, B.; Emtiazi, G. Synthesis and Characterization of a Novel Extracellular Biogenic Manganese Oxide (Bixbyite-like Mn_2O_3) Nanoparticle by Isolated *Acinetobacter* sp. *Curr. Microbiol.* 2011, *63* (3), 300. https://doi.org/10.1007/s00284-011-9971-8.
(47) Akob, D. M.; Bohu, T.; Beyer, A.; Schäffner, F.; Händel, M.; Johnson, C. A.; Merten, D.; Büchel, G.; Totsche, K. U.; Küsel, K. Identification of Mn(II)-Oxidizing Bacteria from a Low-PH Contaminated Former Uranium Mine. *Appl. Environ. Microbiol.* 2014, *80* (16), 5086–5097. https://doi.org/10.1128/AEM.01296-14.
(48) Yang, W.; Zhang, Z.; Zhang, Z.; Chen, H.; Liu, J.; Ali, M.; Liu, F.; Li, L. Population Structure of Manganese-Oxidizing Bacteria in Stratified Soils and Properties of Manganese Oxide Aggregates under Manganese–Complex Medium Enrichment. *PLOS ONE* 2013, *8* (9), e73778. https://doi.org/10.1371/journal.pone.0073778.
(49) Francis, C. A.; Co, E.-M.; Tebo, B. M. Enzymatic Manganese(II) Oxidation by a Marine α-Proteobacterium. *Appl. Environ. Microbiol.* 2001, *67* (9), 4024–4029. https://doi.org/10.1128/AEM.67.9.4024-4029.2001.
(50) Carmichael, M. J.; Carmichael, S. K.; Santelli, C. M.; Strom, A.; Bräuer, S. L. Mn(II)-Oxidizing Bacteria Are Abundant and Environmentally Relevant Members of Ferromanganese Deposits in Caves of the Upper Tennessee River Basin. *Geomicrobiol. J.* 2013, *30* (9), 779–800. https://doi.org/10.1080/01490451.2013.769651.
(51) Poole, R. K. *Microbiology of Metal Ions*; Advances in Microbial Physiology; Elsevier Science, 2017.
(52) Marcus Daniel N.; Pinto Ameet; Anantharaman Karthik; Ruberg Steven A.; Kramer Eva L.; Raskin Lutgarde; Dick Gregory J. Diverse Manganese(II)-oxidizing Bacteria Are Prevalent

633 in Drinking Water Systems. *Environ. Microbiol. Rep.* 2017, *9* (2), 120–128.
634 https://doi.org/10.1111/1758-2229.12508.
635 (53) Takeuchi, M.; Hamana, K.; Hiraishi, A. Proposal of the Genus Sphingomonas Sensu Stricto
636 and Three New Genera, Sphingobium, Novosphingobium and Sphingopyxis, on the Basis
637 of Phylogenetic and Chemotaxonomic Analyses. *Int. J. Syst. Evol. Microbiol.* 2001, *51* (4),
638 1405–1417.
639 (54) Tauler, M.; Vila, J.; Nieto, J. M.; Grifoll, M. Key High Molecular Weight PAH-Degrading
640 Bacteria in a Soil Consortium Enriched Using a Sand-in-Liquid Microcosm System. *Appl.*
641 *Microbiol. Biotechnol.* 2016, *100* (7), 3321–3336. https://doi.org/10.1007/s00253-015-
642 7195-8.
643 (55) Kertesz*, M. A.; Kawasaki, A. Hydrocarbon-Degrading Sphingomonads: Sphingomonas,
644 Sphingobium, Novosphingobium, and Sphingopyxis. In *Handbook of Hydrocarbon and*
645 *Lipid Microbiology*; Timmis, K. N., Ed.; Springer Berlin Heidelberg: Berlin, Heidelberg,
646 2010; pp 1693–1705. https://doi.org/10.1007/978-3-540-77587-4_119.
647 (56) Stumm, W.; Lee, G. F. Oxygenation of Ferrous Iron. *Ind. Eng. Chem.* 1961, *53* (2), 143–
648 146. https://doi.org/10.1021/ie50614a030.
649 (57) Martirani-Von Abercron, S.-M.; Pacheco, D.; Benito-Santano, P.; Marín, P.; Marqués, S.
650 Polycyclic Aromatic Hydrocarbon-Induced Changes in Bacterial Community Structure
651 under Anoxic Nitrate Reducing Conditions. *Front. Microbiol.* 2016, *7*, 1775.
652 https://doi.org/10.3389/fmicb.2016.01775.
653 (58) Eckert, P.; Appelo, C. A. J. Hydrogeochemical Modeling of Enhanced Benzene, Toluene,
654 Ethylbenzene, Xylene (BTEX) Remediation with Nitrate. *Water Resour. Res.* 2002, *38* (8),
655 5–1–5–11. https://doi.org/10.1029/2001WR000692.
656 (59) Emerson, D.; Scott, J. J.; Benes, J.; Bowden, W. B. Microbial Iron Oxidation in the Arctic
657 Tundra and Its Implications for Biogeochemical Cycling. *Appl. Environ. Microbiol.* 2015,
658 *81* (23), 8066–8075. https://doi.org/10.1128/AEM.02832-15.
659 (60) Rose, A. L.; Waite, T. D. Kinetics of Iron Complexation by Dissolved Natural Organic
660 Matter in Coastal Waters. *Mar. Chem.* 2003, *84* (1), 85–103. https://doi.org/10.1016/S0304-
661 4203(03)00113-0.
662 (61) Chen, C.; Thompson, A. Ferrous Iron Oxidation under Varying pO_2 levels: The Effect of
663 Fe^{III}/Al^{III} oxide minerals and organic matter. *Env. Sci. Tech.* 2018, *52*, 597-606.
664 https://doi.org/10.1021/acs.est.7b05102.